Real time Estimation of Projectile Roll Angle using Magnetometers: In-lab Experimental Validation

Changey S., Pecheur E., Wey P., Sommer E.

French-German Research Institute of Saint-Louis (ISL)
P.O. Box 70034, 68301 Saint-Louis, France
sebastien.changey@isl.eu
emmanuel.pecheur@isl.eu
pierre.wey@isl.eu
eckhart.sommer@isl.eu

Abstract

The knowledge of the roll angle of a projectile is decisive to apply guidance and control law. For example, the goal of ISL's project GSP (Guided Supersonic Projectile) is to change the flight path of an air-defence projectile in order to correct the aim error due to the target manoeuvres. The originality of the concept is based on pyrotechnical actuators and onboard sensors which control the angular motion of the projectile. First of all, the control of the actuators requires the precise control of the roll angle of the projectile. To estimate the roll angle of the projectile, two magnetometers are embedded in the projectile to measure the projection of the earth magnetic field along radials axes of the projectiles. Then, an extended Kalman filter is used to compute the roll angle estimation.
As the rolling frequency of the GSP is about 22 Hz, it was easy to test the navigation algorithm in laboratory. In a previous paper [6] the In-Lab demonstration of this concept shows that the roll angle estimation was possible with an accuracy of about 1°. In this paper, the demonstration is extended to high speed roll rate, up to 1000 Hz. Thus, two magnetometers, a DSP and a LED are rotated using a pneumatic motor; the DSP runs an extended Kalman filter and a guidance algorithm to compute the trigger times of the LED. By using a high speed camera, we can observe and improve the accuracy of the method.

1. Guided Supersonic Projectile (GSP)

For ground-based air defence gun systems to be effective, the ability to hit the target is a prerequisite. To achieve high hit probability performance against manoeuvring air targets, such as attack helicopters, cruise missiles or un-manned air vehicles, the basic point is to fire projectiles having short times of flight. However, this solution is limited by the performance of the gun. This paper describes an alternative approach based on guided projectiles with embedded maneuver capabilities.

Figure 1 shows a block diagram of the GSP concept (Guided Supersonic Pro-jectile) designed by ISL [5]. It consists of a supersonic 30 mm finned projectile with on-board navigation sensors and lateral impulse thrusters. The system is designed for very short range air defence (< 5 km).
The initial target tracking and fire control processes are supposed to be per-formed by standard systems. The target is tracked using a battlefield-type air defence radar. The initial flight path of the projectile is determined by the future target position which is extrapolated using a simple linear trajectory model. The gun system is supposed to be a highly effective 40 mm gun.

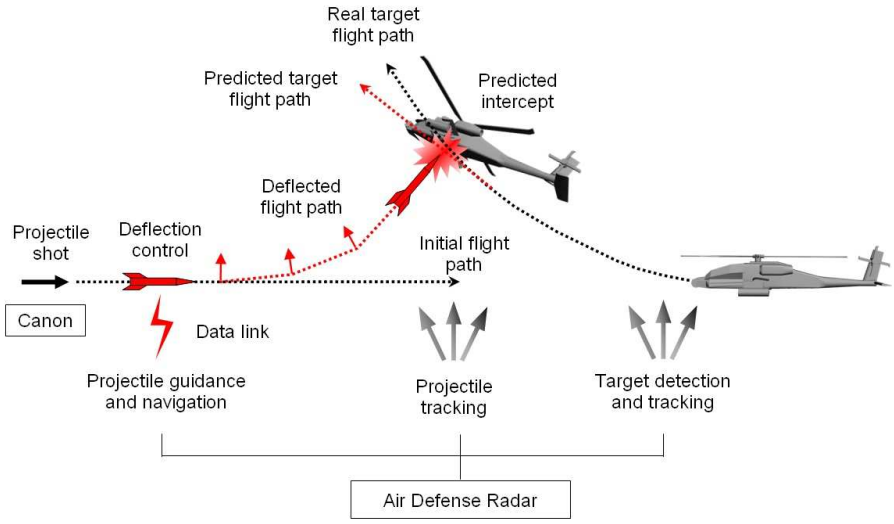

Figure 1: Overview of the GSP concept

After the firing of the projectile, the radar keeps on tracking the target which is supposed to undertake an evasive motion. Its future position is updated using a sequence of tangents at the real trajectory. The radar must also track the projectile in order to estimate the angular deviation required to reach the intercept point.
The angular attitude of the projectile is measured by means of the onboard magnetic sensors designed by ISL [3] and transmitted to the base station. As a matter of fact, the roll angle is needed to trigger the relevant lateral impulse thruster in the direction of the intercept point.
The flight path of the projectile is deflected using a series of near-instantaneous lateral impulses. The effect of a simple lateral impulse has been investigated at the Army Research Laboratory [4]. The original feature of the concept is that the angular motion of the projectile is controlled by series of double impulses in order to sum their effect with the action of the lift force resulting from the angular motion.
The impulse thrusters are small detonators designed by ISL. They are arranged inside the projectile in the form of a ring of lateral divert thrusters. Each of them can deliver an impulse of approximately 1 Ns.

2. Navigation and Control

A two-axis magnetometer sensor is embedded in the projectile (figure 2) to measure the projections of the Earth magnetic field along two radials axis of the body-fixed frame.

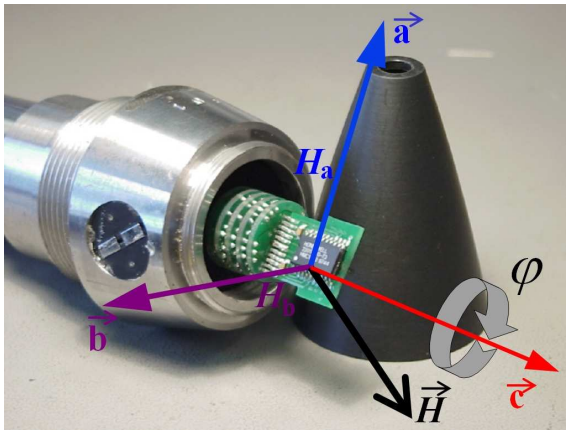

Figure 2: Two magnetometers embedded in the projectile.

By using these 2 measures (H_a, H_b) and the knowledge of the direction of the earth magnetic field in the reference frame $(\vec{H}_{ref})$ an extended Kalman filter is designed to estimate the value of the roll angle φ and the roll rate ω_c. Then, the computation of the trigger time is possible depending on the roll angle estimation $\hat{\varphi}$, the target angle φ_d and the roll velocity estimation $\hat{\omega}_c$.

2.1 Roll angle estimation using an Extended Kalman Filter

To design the Extended Kalman Filter (EKF) used to estimate the roll angle of the projectile, a dynamic modelling was developed [2].

$$\dot{v} = -k_0 v_0^{1/2} v^{3/2} \tag{2.1}$$

$$\omega_c = \dot{\varphi} = v \frac{\varepsilon}{r_f} \tag{2.2}$$

The evolution of the projectile velocity depends on the initial velocity $v_0 \approx 1000 m.s^{-1}$ and on the features of the projectile symbolized by the constant k_0 (2.1). The evolution of the roll angle φ is directly link to the linear velocity (2.2); the fin cant angle ε is about 0.15° and r_f denotes the distance between the axis of the projectile and the centre of the fin.
The modelling of the observation equations is a basic projection of the direction of the Earth magnetic field in the body frame. A complete model requires taking into account the trajectory and the angular motion of the projectile. Since only the estimation of the roll angle φ is needed, some simplifications can be done. So (2.3) represents the observation model, where H_{env} and λ depend on the angular position of the projectile along its trajectory [1]:

$$\begin{cases} H_a = H_{env} \cos(\lambda - \varphi) \\ H_b = H_{env} \sin(\lambda - \varphi) \end{cases} \tag{2.3}$$

According to the sensors model (scale factor and offset) (2.4) represents the complete observation model implemented in the Extended Kalman Filter:

$$Y_{obs} = \begin{bmatrix} L_a H_{env} \cos(\lambda - \varphi) + R_A \\ L_b H_{env} \sin(\lambda - \varphi) + R_B \end{bmatrix} \tag{2.4}$$

As the scale factor (L_A, L_B) and the offset (R_A, R_B) are unknown, it is necessary to estimate them in the EKF, so they are included in the state vector X. According to the projectile's dynamics, an Euler discretization with a sample time $T_e = 1\,ms$ is sufficient. (2.5) represents the evolution model implemented in the Extended Kalman Filter:

$$X_{k+1} = \begin{bmatrix} \varphi \\ \dot{\varphi} \\ v \\ L_A \\ R_A \\ L_B \\ R_B \end{bmatrix}_{k+1} = \begin{bmatrix} \varphi \\ \dot{\varphi} \\ v \\ L_A \\ R_A \\ L_B \\ R_B \end{bmatrix}_k + T_e \begin{bmatrix} \dot{\varphi} \\ \ddot{\varphi} \\ \dot{v} \\ 0 \\ 0 \\ 0 \\ 0 \end{bmatrix}_k = \begin{bmatrix} X_k(1) + T_e\, X_k(2) \\ X_k(2) - T_e\, \varepsilon / r_f\, k_0\, v_0^{1/2}\, X_k(3)^{3/2} \\ X_k(3) - T_e\, k_0\, v_0^{1/2}\, X_k(3)^{3/2} \\ L_A \\ R_A \\ L_B \\ R_B \end{bmatrix} \tag{2.5}$$

The observation model can now be written:

$$Y_k = \begin{bmatrix} X(4)\,H_{env}\cos\big(\lambda - X(1)\big) + X(5) \\ X(6)\,H_{env}\sin\big(\lambda - X(1)\big) + X(7) \end{bmatrix} \tag{2.6}$$

First, the EKF is tested in simulation. Figure 3 shows the estimation of the roll angle $\hat{\varphi}$ and figure 4 shows the estimation of the magnetometer measurements on the axis of the body-fixed frame.

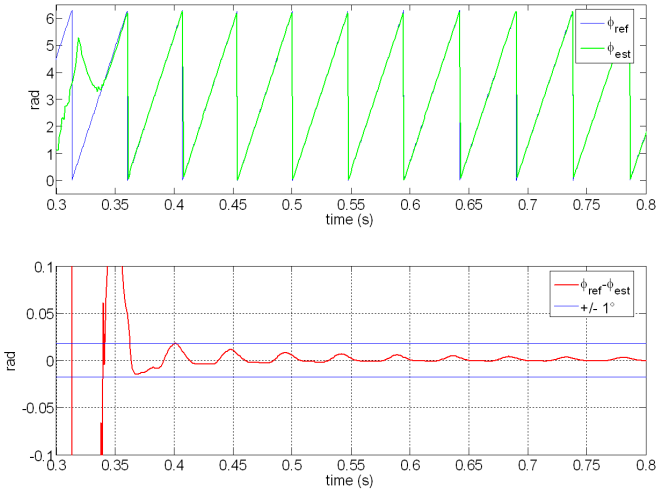

Figure 3: Roll angle estimation.

The previous figures present simulation results of the roll angle estimation. The filter algorithm starts at time t=0.3s when the roll rate has reached its steady state. The figure on the top compares the reference angle with the estimation angle: one revolution seems enough to make the estimation converge. The figure on the bottom focus on the estimation error: after 0.1s the estimation error stays under 1°. So, the reference and estimation angles are close enough to have a good precision on the trigger estimation time.

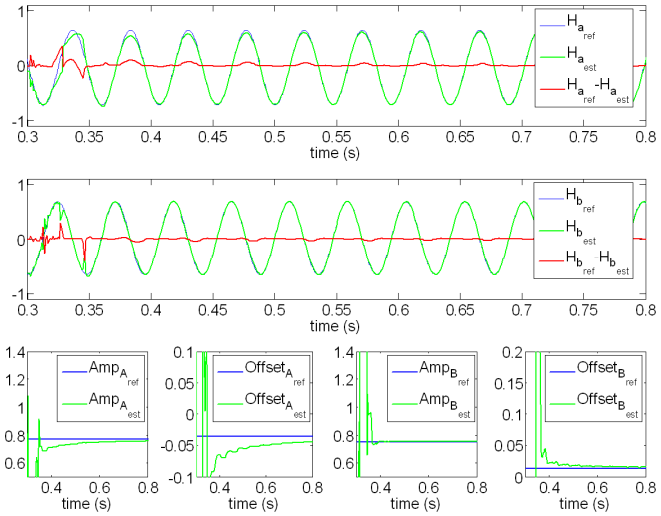

Figure 4: Magnetometers measurements estimation.

No direct measurement of the roll angle is available on the experiment system. Thus, to test and validate our method, we compare the magnetometer measurements and estimates. The magnetometer estimates $H_{a\,est}$ and $H_{b\,est}$ are computed from the estimation state vector (2.7).

$$\begin{cases} H_{a\,est} = \hat{X}(4)\,H_{env}\cos\left(\lambda - \hat{X}(1)\right) + \hat{X}(5) \\ H_{b\,est} = \hat{X}(6)\,H_{env}\sin\left(\lambda - \hat{X}(1)\right) + \hat{X}(7) \end{cases} \quad \textbf{(2.7)}$$

Figure 4 shows simulation results for the estimations of the scale factors and the offsets of the two embedded magnetometers. These four estimates converge on the simulated values. On the top figure, the estimation of the magnetometer measure $H_{a\,est}$ and $H_{b\,est}$ converges to the simulated references signals $H_{a\,ref}$ and $H_{b\,ref}$; the simulation shows that only one revolution is enough to have a good accuracy.

2.2 Trigger time prediction

Considering the small size of the projectile, the computation of the algorithm on a DSP cannot be embedded. So, a HF transmission between a base station and the projectile is necessary. First, sensors values are sent to the base station. Then, after the DSP computation process, the impulse trigger time is sent back to the projectile.
The impulse trigger time t_{imp} is predicted from the state estimated vector, the target roll angle and the embedded clock time (2.8) and (2.9).

$$t_{imp} = t + \frac{\left(\varphi_t - \hat{\varphi}\right)}{\hat{\omega}_c} \quad \textbf{(2.8)}$$

$$t_{imp} = t + \frac{\left(\varphi_t - \hat{X}(1)\right)}{\hat{X}(2)} \quad \textbf{(2.9)}$$

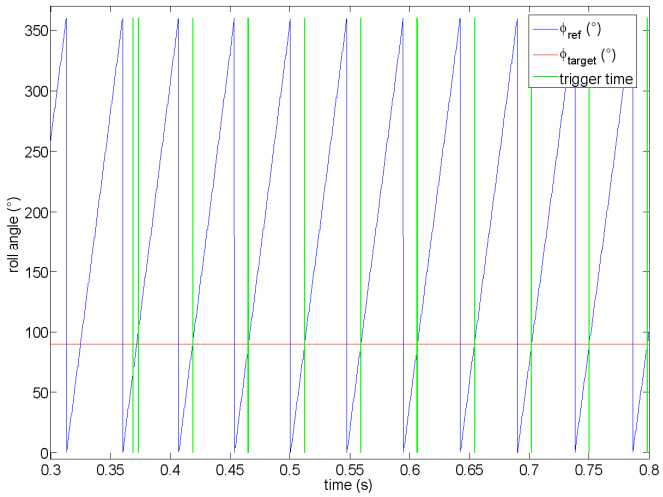

Figure 5: Predicted trigger time for φ_t =90°.

For example, figure 5 shows the trigger time computed for a target roll angle of 90°. As a new predicted trigger time is computed, the new value is sent to the projectile to update the previous value. Considering the 22 Hz roll rate and the 1 ms sample time, the trigger time can be updated up to 40 times per revolution.
The results presented on the figure show us that only the first predicted trigger time is wrong, due to the delay imposed by the convergence of the algorithm.

3. In-Lab experimental validation

3.1 Design of the test bench

We developed a test bench according to constraints for the actuators:

- The motor has to reach a high speed roll rate.
- The actuator should not disturb the magnet field, that's why we cannot use an electric motor.
- The motor and the electronic module have to be mounted into a safety box.

We decided to use a pneumatic motor. The pneumatic motor we chose has a maximum no load speed up to 70000 rpm (revolution per minute) under a pressure of 90 PSI (6 bar). This kind of motors are designed for grinding (with tools up to a diameter of 3 mm only), that's why a lot of preliminary tests has been done to make sure we are able to spin a much larger cylinder : 38mm diameter, 90mm long, weight above 140g.

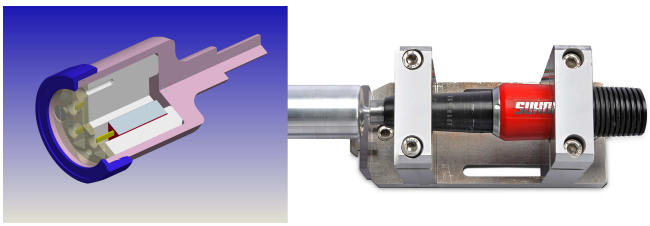

Figure 6: Shell on which the electronic module is embedded

The motor has been inserted in a polycarbonate box. This box is transparent so we can place a high-speed camera in front of the LED to observe the behavior of the roll rate estimation.

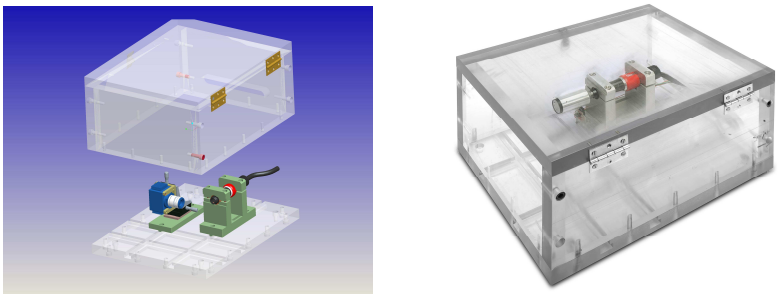

Figure 7: CAD view of the test bench and the manufactured one

The electronic module has been tested with this high speed rotation and no damages or dysfunctions have been detected.

3.2 Experimental results

We used a high speed camera with an acquisition speed up to 250 000 frames per second. In our case the rotation frequency we reached was about 950 Hz. The images have been processed to find the pictures on which the LED is switched on. A picture can be seen as a matrix with RGB levels. The white color has the highest value which is 255. A First method could be, finding the value 255 within a picture to isolate the picture with light on. This cannot work because there is noise on the pictures. Our method was to calculate the mean value of each matrix. So the pictures on which the light is switched on correspond to the highest mean values.

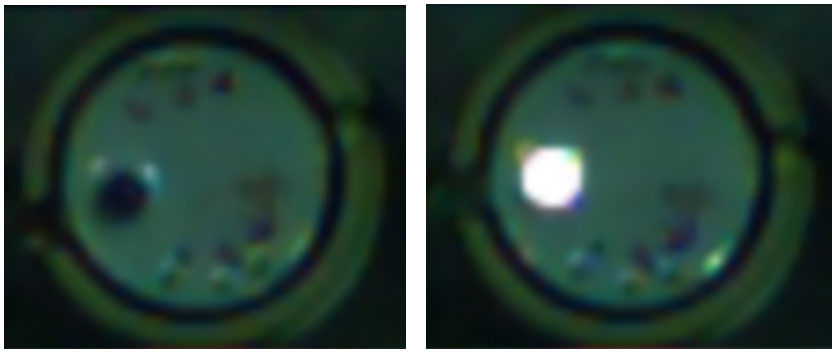

Figure 8: Pictures obtained with the high-speed camera.

The mean values of the pictures on which the light is on are higher than 50 while in the other case the mean values are between 32 and 37. A threshold value allows us to extract the wanted pictures.

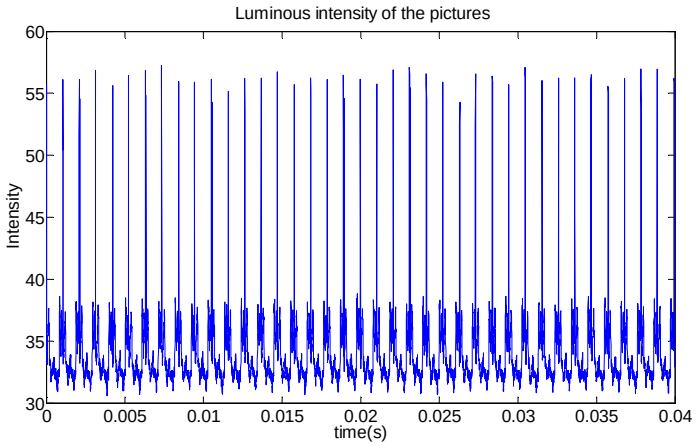

Figure 9: Mean value of each picture.

A study of the roll frequency shows that the value is not constant during the 2 s of the measurement. At the beginning the frequency is 951 Hz and at the end near to 949 Hz. The medium value is 950.46 Hz. This variation converted to a time spread (2.21 µs) and then to the angular orientation leads to an error of 0.75°. We first consider that this error is negligible.

The second step was to determine the time between successive trigger events of the LED in order to quantify the jitter.

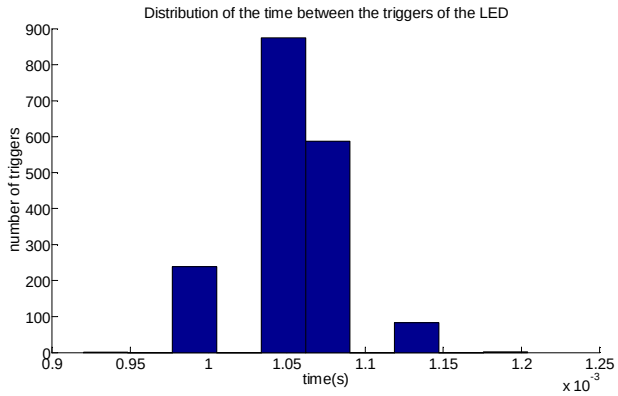

Figure 10: Distribution of the time between the trigger of the LED.

First result leads us to a standard deviation of up to 30 µs which means for this frequency, a precision of about 10°.
The Kalman filter we developed was not specifically designed to be only used at a 1000 Hz roll rate. We first wanted to scan a range between 100 and 1000Hz with the same filter.
In a previous study we had made some experiment on our filter by simulating the magnetometer signals with a function generator. The maximal standard deviation we obtained was less than 1° over all this frequency range. That's why we expect to improve the accuracy of our algorithm.

3.3 Conclusion and outlooks

The hardware we developed resists to the high speed rotation. The first results have shown the accuracy of the roll angle estimation is not as expected. We need to investigate in order to reduce the standard deviation. For that we will embed a recorder and process those data to see if the errors come from the algorithm or from the software clock that generates the trigger events.

References

[1] Changey, S. 2005. Modélisation et estimation par filtrage non linéaire de l'attitude d'un projectile à partir de magnétomètres. *Supélec Phd Thesis. France.*
[2] Fleck, V. 1998. Introduction a la Balistique Extérieure. *Institut Franco-Allemand de Recherche de Saint-Louis. France*
[3] Fleck, V., Meyer, R., Sommer, E. 2004. Onboard Measurements of the Motion of Projectiles with Accelerometers and Magnetometers. *21st International Symposium on Ballistics. Adelaide, Australia.*
[4] Guidos, B. J., Cooper, G. R. 1999. The Effect of a Simple Lateral Impulse on Kinetic Energy Projectile in Flight. *Army Research Laboratory. Report ARL-TR-2076*
[5] Wey, P., Berner, C., Sommer, E., Fleck, V. and Moulard, H. 2005. Theoretical Design for a Guided Supersonic Projectile. *22th International Symposium on Ballistics. Vancouver, BC, Canada.*
[6] Changey, S., Pecheur, E., Wey, P. 2009. Real-Time Estimation of Supersonic Projectile Roll Angle Using Magnetometers: In-lab Experimental Validation. *2nd IFAC Workshop on Dependable Control of Discrete Systems, Bari, IT, June 10-12, 2009. Bari, Italy.*